First-principles study on thermoelectric properties of half-Heusler compounds CoMSb (M = Sc, Ti, V, Cr, and Mn)

Susumu Minami (iD), Fumiyuki Ishii, Yo Pierre Mizuta, and Mineo Saito

View Online   Export Citation   CrossMark

ARTICLES YOU MAY BE INTERESTED IN

First-principles study on thermoelectric properties of half-Heusler compounds CoMSb (M = Sc, Ti, V, Cr, and Mn)

Susumu Minami,[1,a)] Fumiyuki Ishii,[2,b)] Yo Pierre Mizuta,[1] and Mineo Saito[2]

[1]Graduate School of Natural Science and Technology, Kanazawa University, Kakuma, Kanazawa 920-1192, Japan
[2]Faculty of Mathematics and Physics, Institute of Science and Engineering, Kanazawa University, Kakuma, Kanazawa 920-1192, Japan

We have performed systematic density functional calculations and evaluated thermoelectric properties (Seebeck coefficient and anomalous Nernst coefficient) of half-Heusler compounds CoMSb (M = Sc, Ti, V, Cr, and Mn). The carrier concentration dependence of the Seebeck coefficient in nonmagnetic compounds is in good agreement with experiments. We found that the half-metallic ferromagnetic CoMnSb shows a large anomalous Nernst effect originating from Berry curvature near the Brillouin zone boundary. These results help us understand the mechanism of a large anomalous Nernst coefficient and give us a clue to design high performance magnetic thermoelectric materials. *Published by AIP Publishing.* https://doi.org/10.1063/1.5029907

The Nernst effect induces a thermoelectric (TE) voltage under a magnetic field. The direction of the TE voltage is perpendicular to the thermal gradient, which can be exploited to modularize TE generation devices.[1] Unlike the conventional Nernst effect, the anomalous Nernst effect (ANE)[2–4] does not require an external magnetic field and is induced by spontaneous magnetization. Because the TE voltage from ANE appears perpendicularly to the thermal gradient, ANE has several unique technological benefits and is expected as a new mechanism for TE generation systems.[5]

To realize widespread use of ANE-based TE generation devices, a large anomalous Nernst coefficient is needed.[5] However, the reported anomalous Nernst coefficient N [$\leq 1\,\mu$V/K (Refs. 6–11)] is two orders of magnitude smaller than the Seebeck coefficient S [$\sim 10^2\,\mu$V/K (Refs. 12 and 13)] in typical TE materials. The ANE magnitude can be enhanced either by strong asymmetry of the anomalous Hall conductivity along the energy axis or by a large product of the Seebeck coefficient and Hall angle ratio.[14,15] This implies that large ANE could be found in magnetic materials with a large anomalous Hall effect and/or large Seebeck effect. Here, we focus on half-Heusler compounds, which are known as conventional TE materials, because of expectation for the contribution of the large Seebeck effect to ANE.

Half-Heusler compounds are candidate materials for ANE-based TE devices. Such compounds are known to be good TE materials with a large Seebeck effect originating from their narrow-gap semiconducting state with 18 valence electron count per formula unit (f.u.).[16] For example, CoTiSb and NiTiSn show large S values of -320 and $-250\,\mu$V/K at 300 K, respectively.[17,18] Half-Heusler compounds are also well known as half-metallic ferromagnets with high Curie temperature.[19] For example, CoMnSb and NiMnSb show ferromagnetism with Curie temperatures of 490 and 730 K, respectively.[20] Therefore, large ANE could be realized by tuning the electron or hole carrier density of half-Heusler compounds.

In this study, we investigate the TE properties of half-Heusler compounds with the formula CoMSb (M = Sc, Ti, V, Cr, and Mn). We perform first-principles calculations for these compounds. We calculate the TE properties based on the obtained electronic structures. We estimate the carrier concentration dependence of the Seebeck coefficient by using semiclassical Boltzmann transport theory. To clarify the ANE of ferromagnetic half-Heusler compounds, we focus on CoMnSb and estimate both the anomalous Nernst coefficient and the Seebeck coefficient.

Figure 1 shows the schematic structure of CoMSb. Half-Heusler intermetallic compounds have a face-centered cubic crystal structure with chemical composition XYZ and space group $F\bar{4}3m$. The atomic sites in the unit cell $X\left(\frac{1}{4}, \frac{1}{4}, \frac{1}{4}\right)$, $Y(0,0,0)$, and $Z\left(\frac{1}{2}, \frac{1}{2}, \frac{1}{2}\right)$ are occupied. The X atomic site is coordinated doubly tetrahedrally by four Y and four Z. Therefore, the X site is regarded as the unique site in the crystal structure. Table I shows the lattice constant, valence electron count, and Curie temperature of CoMSb. Because no
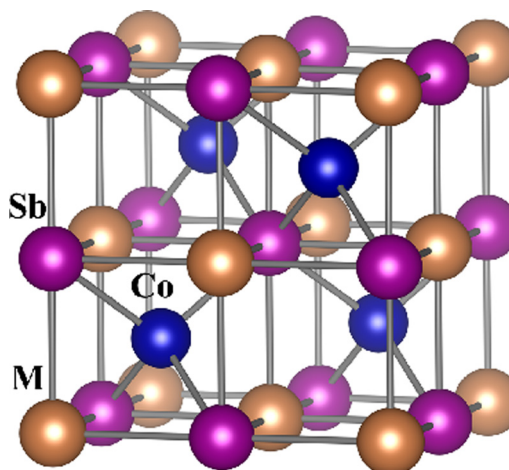

FIG. 1. Schematic structure of the half-Heusler compounds CoMSb.

a)Electronic mail: minami@cphys.s.kanazawa-u.ac.jp
b)Electronic mail: fishii@mail.kanazawa-u.ac.jp

TABLE I. Basic properties of Co*M*Sb. a_{exp} and a_{cal} are the experimental and theoretical lattice constants, n_v is the number of valence electrons per f.u., and T_C is the Curie temperature. Our calculation was performed by using a we estimated.

M	a (Å)	$a_{exp.}$ (Å)	a_{calc} (Å)	n_v	T_C (K)
Sc	6.06	…	6.09 (Ref. 22)	17	…
Ti	5.88	5.88 (Ref. 23)	5.88 (Ref. 24)	18	…
V	5.80	5.80 (Ref. 25)	5.81 (Ref. 24)	19	58 (Ref. 21)
Cr	5.79	…	5.79 (Ref. 22)	20	…
Mn	5.87	5.87 (Ref. 26)	5.82 (Ref. 24)	21	490 (Ref. 20)

experimental lattice constants have been reported for Sc and Cr, we used interpolated ones calculated based on those of $M = $ Ti, V, and Mn. CoTiSb is a semiconductor with 18 valence electron count and a narrow gap. CoVSb and CoMnSb are ferromagnetic compounds with Curie temperatures of 58 K and 490 K, respectively.[20,21]

We conducted first-principles calculations based on the non-collinear density functional theory[27] (DFT) with OpenMX code.[28] DFT calculations are performed through the exchange-correlation functional of the generalized gradient approximation.[29] We used norm-conserving pseudopotentials.[30] The spin-orbit interaction (SOI) is included by using j-dependent pseudopotentials.[31] The wave functions are expanded by a linear combination of multiple pseudo-atomic orbitals.[32] The basis functions of each atom are two s-, two p-, two d-, and one f- character numerical pseudo-atomic orbitals. The cutoff-energy for charge density is 250.0Ry. We use a $24 \times 24 \times 24$ uniform k-point mesh for self-consistent calculations. We construct maximally localized Wannier functions (MLWFs) from DFT calculation results using the Wannier90 code[33] and calculate the transport properties from the MLWF by using the semiclassical Boltzmann transport theory.[34]

The formulae for the TE coefficients can be derived from the linear response relation of charge current, $\boldsymbol{j} = \tilde{\sigma}\boldsymbol{E} + \tilde{\alpha}(-\nabla T)$, where $\boldsymbol{E}$ and ∇T are the electric field and temperature gradient, respectively,. By using the conductivity tensors $\tilde{\sigma} = [\sigma_{ij}]$ and $\tilde{\alpha} = [\alpha_{ij}]$, the Seebeck and anomalous Nernst coefficients are, respectively, expressed as[14,15]

$$S \equiv S_{xx} \equiv \frac{E_x}{(\nabla T)_x} = \frac{S_0 + \theta_H N_0}{1 + \theta_H^2}, \quad (1)$$

$$N \equiv S_{xy} \equiv \frac{E_x}{(\nabla T)_y} = \frac{N_0 - \theta_H S_0}{1 + \theta_H^2}. \quad (2)$$

Here, we defined the conventional (pure) Seebeck, Hall angle ratio, and pure anomalous Nernst coefficient by using the conductivity tensors as follows: $S_0 \equiv \alpha_{xx}/\sigma_{xx}$, $\theta_H \equiv \sigma_{xy}/\sigma_{xx}$, $N_0 \equiv \alpha_{xy}/\sigma_{xx}$. The longitudinal conductivity tensor is calculated as $\sigma_{xx} = e^2\tau \sum_n \int d\boldsymbol{k} v_x^n(\boldsymbol{k})^2 \left(-\frac{\partial f}{\partial \varepsilon_{n\boldsymbol{k}}}\right)$, and the transverse conductivity tensor is calculated as $\sigma_{xy} = -\frac{e^2}{\hbar} \sum_n \int d\boldsymbol{k}\, \Omega_z^n(\boldsymbol{k}) f(\varepsilon_{n\boldsymbol{k}})$. Both the longitudinal and transverse TE conductivity tensors are calculated as $\alpha_{ij} = \frac{1}{e} \int d\varepsilon \sigma_{ij}(\varepsilon)|_{T=0} \frac{\varepsilon-\mu}{T}\left(-\frac{\partial f}{\partial \varepsilon}\right)$. In the above formula, $\tau, f, v_x^n, \varepsilon_{n\boldsymbol{k}}, \Omega_z^n$, and μ denote the relaxation time (assumed to take constant value τ), Fermi-Dirac distribution function, group velocity of

electrons, energy and $\boldsymbol{k}$-space Berry curvature, and chemical potential, respectively. The Berry curvature is determined by $\boldsymbol{\Omega}^n(\boldsymbol{k}) \equiv i\langle \boldsymbol{\nabla_k} u_{n\boldsymbol{k}} | \times | \boldsymbol{\nabla_k} u_{n\boldsymbol{k}} \rangle$. The subscript n is the band index. Note that the conventional Seebeck coefficient S_0 is calculated by setting $\theta_H = 0$ and $N_0 = 0$ in Eq. (1). We focus on the intrinsic contribution of σ_{xy} and neglect the extrinsic ones caused by impurities or defects. Here, in order to discuss the chemical potential (μ) dependence of TE coefficients, we introduce Mott's formula, $S_0 \simeq \alpha_{xx}^{(1)}/\sigma_{xx}$, $N_0 \simeq \alpha_{xy}^{(1)}/\sigma_{xx}$, where $\alpha_{ij}^{(1)}$, defined as $\alpha_{ij}^{(1)}(\mu) \equiv -\frac{\pi^2}{3}\frac{k_B^2 T}{e}\frac{\partial \sigma_{ij}(\varepsilon)}{\partial \varepsilon}|_{\varepsilon=\mu}$ with Boltzmann's constant k_B, is the low T approximation to α_{ij}.

Because N_0 and θ_H are zero for nonmagnetic materials (CoScSb and CoTiSb) and the nonmagnetic (paramagnetic) phase of CoVSb, CoCrSb, and CoMnSb, we first calculate the conventional (pure) Seebeck coefficient S_0.

Figure 2 shows the electronic structure, density of states (DOS), and electrical conductivity at 0 K of CoTiSb. The calculated bandgap for 1.06 eV is in good agreement with the experimental bandgap of 0.95 eV.[35] The Fermi energies (E_F) are calculated by the rigid band approximation (RBA) for other half-Heusler compounds, namely, CoScSb, CoVSb, CoCrSb, and CoMnSb.

Figure 3 shows carrier concentration dependence of S_0, which is estimated by two approaches: (i) RBA in CoTiSb and (ii) self-consistent field (SCF) calculation by hole- or electron- doping around each pristine Co*M*Sb. The trends of the carrier concentration dependence of S_0 are broadly consistent between RBA and SCF.

Positive (negative) S_0 values are observed on the left (right) side of CoTiSb in Fig. 3, which can be attributed to the hole- (electron-) doped semiconductor, respectively. The S_0 values of 0.05e/f.u. hole- and electron-doped CoTiSb calculated by RBA are 138 μV/K and -125 μV/K, respectively; these are in good agreement with the experimental values of 178 μV/K and -163 μV/K observed in CoTi$_{0.95}$Sc$_{0.05}$Sb and CoTi$_{0.95}$V$_{0.05}$Sb, respectively.[36] On the other hand, the Seebeck coefficient calculated by SCF of CoVSb is around three times larger than the calculated RBA, which is much closer to the experimental value[37] of -45 μV/K.

The trend of the carrier concentration dependence of S_0 can be roughly interpreted using Mott's formula. Because
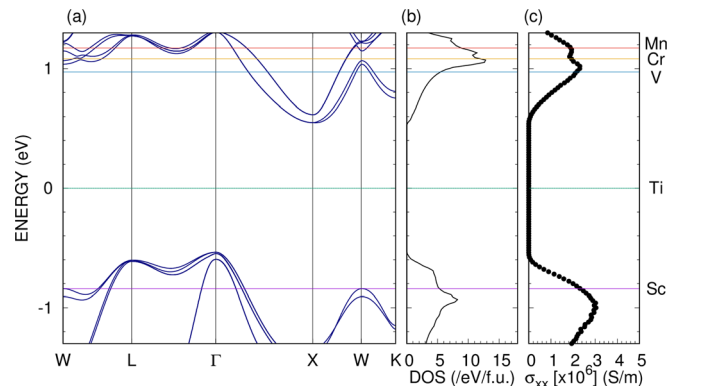

FIG. 2. Band structure (a), density of states (b), and electrical conductivity at 0 K with a relaxation time of $\tau = 10$ fs (c) of CoTiSb. The origin of the energy is taken at the Fermi energy of CoTiSb. The colored lines show the Fermi energy of Co*M*Sb according to the rigid band approximation.
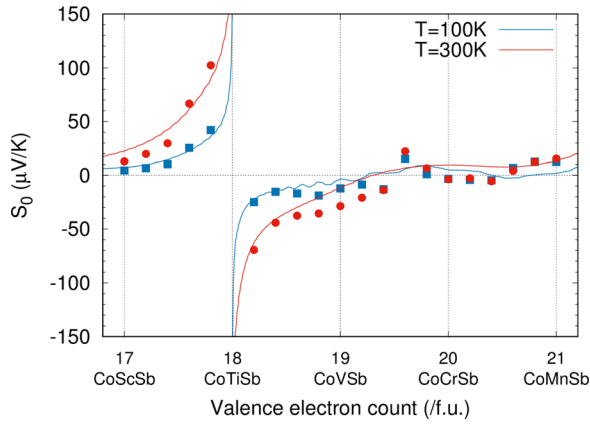
FIG. 3. Valence electron count dependence of the Seebeck coefficient in CoMSb at 100 K and 300 K. The solid lines show the Seebeck coefficient according to rigid band approximation. Squares and circles show the Seebeck coefficient calculated by using the electronic structure with the self-consistent field calculation.

σ_{xx} at E_F of CoScSb, CoCrSb, and CoMnSb has a negative slope in Fig. 2(c), $\alpha_{xx}^{(1)}$ is positive. On the other hand, because σ_{xx} at E_F of CoVSb has a positive slope, $\alpha_{xx}^{(1)}(E_F)$ is negative. For $M = $ Cr, the sign of S_0 between RBA and SCF is different, implying that RBA using the band structure of CoTiSb is not appropriate for CoCrSb.

We investigate CoMnSb because of its applicability for ANE-based TE modules that can operate above room temperature. Figure 4 shows the band structure and DOS for CoMnSb. At the Fermi level, the majority (minority) spin shows an electron- (hole-) like band structure around the X (Γ) point in Figs. 4(a) and 4(b). A comparison of the DOS at E_F of the nonmagnetic and ferromagnetic phases in Figs. 2(b) and 4(c) indicates that the ferromagnetic phase has smaller $D(E_F) \sim 2$/eV/f.u. than $D(E_F) \sim 9$/eV/f.u. in the nonmagnetic phase. This change in $D(E_F)$ can be attributed to ferromagnetic phase transition induced by Stoner instability. The total magnetic moment is $\sim 3\,\mu_B$/f.u. Moreover, the obtained atomic magnetic moments of Co, Mn, and Sb are -0.3, 3.6, and $-0.3\,\mu_B$/f.u., respectively.

TABLE II. Each component of the calculated thermoelectric coefficients (μV/K), Hall angle ratio, and evaluated relaxation time (fs) for CoMnSb at Fermi energy ($\mu = 0$).

Temperature (K)	S_0	N_0	$\theta_H[\times 10^{-2}]$	S	N	τ[a]
100	-5.80	-0.11	-0.42	-5.79	-0.13	7.0
300	-16.00	-0.85	-1.02	-15.99	-1.02	2.9

[a]τ is estimated as $\tau = \tau_0(\rho_{calc}/\rho_{exp})$, where $\rho_{calc} = 1/\sigma_{xx}(\tau_0)$ is the calculated electrical resistivity and ρ_{exp} is the experimental one reported in Ref. 20.

Table II shows the TE properties of CoMnSb at E_F. We found unique TE properties in the ferromagnetic phase: the ferromagnetic phase shows negative S, whereas the nonmagnetic phase shows positive S (Fig. 3). A large anomalous Nernst coefficient (N) that reaches $-1.02\,\mu$V/K at 300 K was also found; this value is fairly large compared to that of the reported ferromagnetic metals, for example, $\sim 0.6\,\mu$V/K for the L1$_0$-ordered FePt thin film.[6] The main component of N [referring to Eq. (2)] is the pure anomalous Nernst coefficient (N_0). The contributions of two components N_0 and $S_0\theta_H$ are $\sim 80\%$ and $\sim 20\%$, respectively.

To understand the unique TE properties in the ferromagnetic phase of CoMnSb, we show the chemical potential dependence of the TE coefficient at 100 and 300 K and the electrical conductivity at 0 K in Figs. 5 and 6, respectively. First, we discuss the Seebeck coefficient (S). The negative sign of S at E_F can be understood from Mott's formula: $\alpha_{xx}^{(1)}(E_F)$ is negative because $\sigma_{xx}(E_F)$ has a positive slope, as shown in Fig. 6(a). The peak of S in Fig. 5(a) is around E_F, and the maximum is $\sim 15\,\mu$V/K at 300 K, which is not so large compared with that of typical TE materials. Next, we discuss the anomalous Nernst coefficient (N). N shows two peaks in Fig. 5(b) at the lower- and higher-energy sides of $\mu_P \equiv -85$ meV. The chemical potential of μ_P is indicated by the vertical dotted line in Figs. 5 and 6. For N, the two peaks show opposite signs owing to the almost-even functional form $\sigma_{xy}(\varepsilon - \mu_P) \simeq \sigma_{xy}(-\varepsilon + \mu_P)$ in Fig. 6(b), leading to the almost-odd functional form of its first derivative, to which $\alpha_{xy}^{(1)}$ is proportional as shown in Mott's formula.
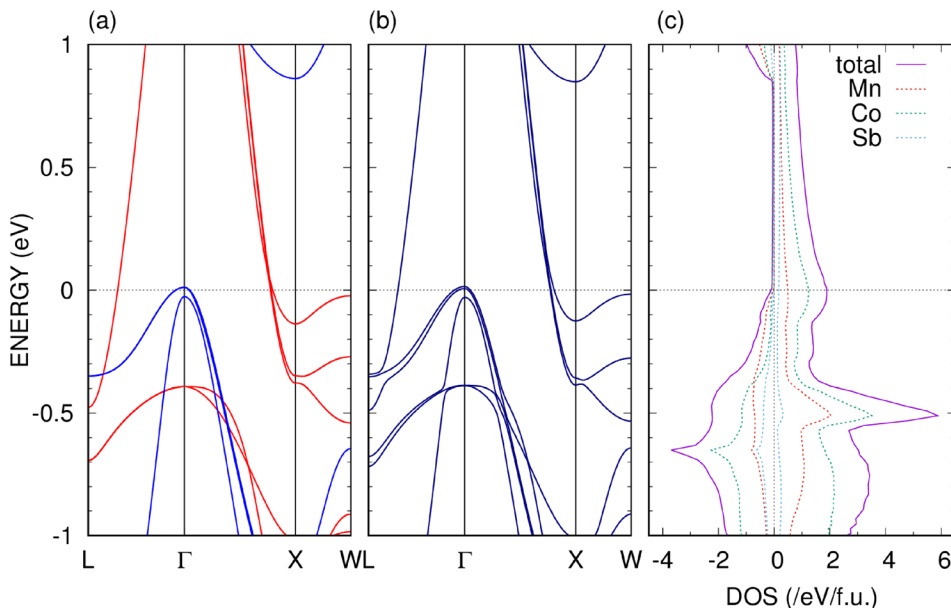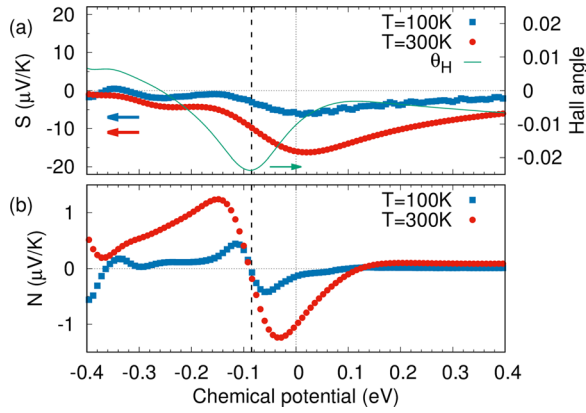

FIG. 4. Band structure of CoMnSb without SOI (a), with SOI (b), and total and projected density of states for CoMnSb (c). Red and blue lines show the majority and minority spins, respectively. The Fermi energy is set to 0 eV.

FIG. 5. Thermoelectric properties for CoMnSb at 100 K and 300 K. Each panel shows the Seebeck coefficient and Hall angle ratio (300 K) (a) and anomalous Nernst coefficient (b).

To clarify the origin of negative peak $\sigma_{xy}(\mu_P)$, we focus on the band structure and iso-energy surface at μ_P because in general large σ_{xy} comes from energy splittings in time-reversal-symmetry-breaking electronic bands induced by SOI in ferromagnetic states.[38,39] The anomalous Hall conductivity and Berry curvature are calculated as $\sigma_{xy} = -\frac{e^2}{\hbar}\sum_n \int d\boldsymbol{k}\, \Omega_z^n(\boldsymbol{k})f(\varepsilon_{nk})$ and $\Omega_z^n(\boldsymbol{k}) = -2\mathrm{Im}\sum_{m\neq n}\frac{v_{nm,x}(\boldsymbol{k})v_{mn,y}(\boldsymbol{k})}{[\varepsilon_m(\boldsymbol{k})-\varepsilon_n(\boldsymbol{k})]^2}$, respectively.[40] Here, $v_{nm,\alpha}(\boldsymbol{k})$ is the matrix elements of the Cartesian velocity. This expression of Berry curvature, which is proportional to the inverse of the energy difference, suggests that large σ_{xy} comes from avoided crossings of the energy bands caused by SOI. Figure 7(a) shows the band structure along the symmetry lines in the part of Brillouin zone where large Berry curvature was found ($k_z = 2\pi/a$ plane). A small energy splitting originating from SOI is found on the $Z\left(0,0,\frac{2\pi}{a}\right) - Uz\left(\frac{\pi}{2a},\frac{\pi}{2a},\frac{2\pi}{a}\right)$ line.

The iso-energy surface and summed Berry curvature around $Z\left(0,0,\frac{2\pi}{a}\right)$ are shown in Figs. 7(b) and 7(c), respectively. While we assumed the magnetic easy axis as the [001] direction in a cubic system, the calculated easy axis of magnetization is slightly tilted from the [001] direction. The weak asymmetry of the Berry curvature in Fig. 7(c) is
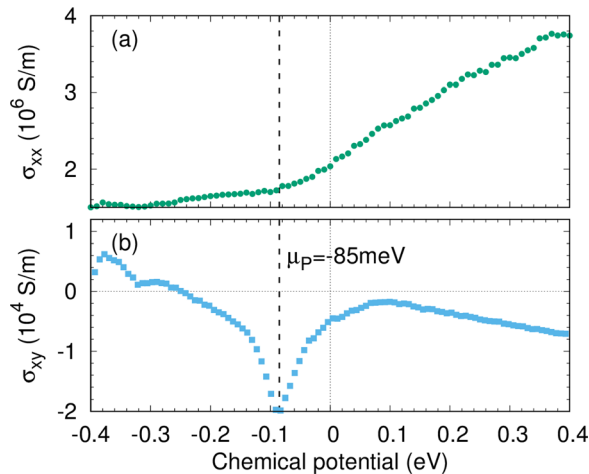

FIG. 6. Chemical potential dependence of electrical conductivity σ_{xx}(S/m) at 0 K with relaxation time $\tau = 10$ fs (a) and anomalous Hall conductivity σ_{xy}(S/m) at 0 K (b).
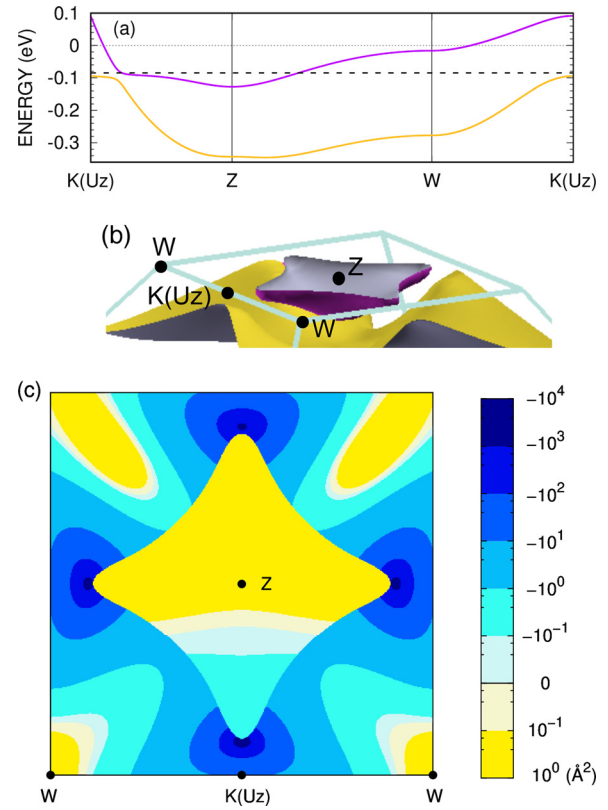

FIG. 7. Band structure with SOI (a), iso-energy surface for $\varepsilon = -85$ meV (b), and sum of Berry curvature over occupied states $\bar{\Omega}_k \equiv \sum_n -\Omega_z^n(\boldsymbol{k})f_n(\varepsilon)$ on the $k_z = \frac{2\pi}{a}$ plane (c) for CoMnSb.

induced by the slight tilting of magnetization. Largely negative summed Berry curvature ($\bar{\Omega}_k \sim -10^4$) appears near $Uz\left(\frac{\pi}{2a},\frac{\pi}{2a},\frac{2\pi}{a}\right)$. This peak shows that the summed Berry curvature changes discontinuously at these boundaries, indicating that the upper band [corresponding to the purple one in Fig. 7(a)] has large positive Berry curvature. Furthermore, it can be predicted that lower band [corresponding to the yellow one in Fig. 7(a)] has large negative Berry curvature. It is obvious that the peak of N and σ_{xy} results from such a change in the Berry curvature on the $Z\left(0,0,\frac{2\pi}{a}\right) - Uz\left(\frac{\pi}{2a},\frac{\pi}{2a},\frac{2\pi}{a}\right)$ line.

In summary, systematic DFT calculations are used to determine the carrier concentration dependence of the TE properties in CoMSb (M = Sc, Ti, V, Cr, and Mn). In the nonmagnetic phase, the calculated Seebeck coefficient of 0.05e/f.u. hole and electron-doped CoTiSb shows good agreement with the experimental data of CoTi$_{0.95}$Sc$_{0.05}$Sb and CoTi$_{0.95}$V$_{0.05}$Sb. In the ferromagnetic phase, we focus on half-metallic CoMnSb because of its high T_C. The Seebeck coefficient shows opposite sign to that in the nonmagnetic phase. Furthermore, the large anomalous Nernst coefficient (N) reaches $-1.02\,\mu$V/K. We conclude that the peaks of N originate from the large Berry curvature on the Z-Uz line. These results should help in understanding the mechanism of large ANE in half-Heusler compounds.

[1] Y. Sakuraba, K. Hasegawa, M. Mizuguchi, T. Kubota, S. Mizukami, T. Miyazaki, and K. Takanashi, Appl. Phys. Express **6**, 033003 (2013).

[2] D. Xiao, Y. Yao, Z. Fang, and Q. Niu, Phys. Rev. Lett. **97**, 026603 (2006).

[3] N. Nagaosa, J. Sinova, S. Onoda, A. H. MacDonald, and N. P. Ong, Rev. Mod. Phys. **82**, 1539 (2010).

[4] D. Xiao, M.-C. Chang, and Q. Niu, Rev. Mod. Phys. **82**, 1959 (2010).

[5] Y. Sakuraba, Scr. Mater. **111**, 29 (2016).

[6] K. Hasegawa, M. Mizuguchi, Y. Sakuraba, T. Kamada, T. Kojima, T. Kubota, S. Mizukami, T. Miyazaki, and K. Takanashi, Appl. Phys. Lett. **106**, 252405 (2015).

[7] W.-L. Lee, S. Watauchi, V. L. Miller, R. J. Cava, and N. P. Ong, Phys. Rev. Lett. **93**, 226601 (2004).

[8] T. Miyasato, N. Abe, T. Fujii, A. Asamitsu, S. Onoda, Y. Onose, N. Nagaosa, and Y. Tokura, Phys. Rev. Lett. **99**, 086602 (2007).

[9] Y. Pu, D. Chiba, F. Matsukura, H. Ohno, and J. Shi, Phys. Rev. Lett. **101**, 117208 (2008).

[10] S. Y. Huang, W. G. Wang, S. F. Lee, J. Kwo, and C. L. Chien, Phys. Rev. Lett. **107**, 216604 (2011).

[11] M. Ikhlas, T. Tomita, T. Koretsune, M. Suzuki, N. Daisuke, R. Arita, Y. Otani, and S. Nakatsuji, Nat. Phys. **13**, 1085 (2017).

[12] G. Chen, M. S. Dresselhaus, G. Dresselhaus, J.-P. Fleurial, and T. Caillat, Int. Mater. Rev. **48**, 45 (2003).

[13] L. Huang, Q. Zhang, B. Yuan, X. Lai, X. Yan, and Z. Ren, Mater. Res. Bull. **76**, 107 (2016).

[14] Y. P. Mizuta and F. Ishii, JPS Conf. Proc. **3**, 017035 (2014).

[15] Y. Mizuta and F. Ishii, Sci. Rep. **6**, 28076 (2016).

[16] T. Graf, C. Felser, and S. S. Parkin, Prog. Solid State Chem. **39**, 1 (2011).

[17] Y. Stadnyk, Y. Gorelenko, A. Tkachuk, A. Goryn, V. Davydov, and O. Bodak, J. Alloys Compd. **329**, 37 (2001).

[18] S. Bhattacharya, A. L. Pope, R. T. Littleton IV, T. M. Tritt, V. Ponnambalam, Y. Xia, and S. J. Poon, Appl. Phys. Lett. **77**, 2476 (2000).

[19] C. J. Palmstrm, Prog. Cryst. Growth Charact. Mater. **62**, 371 (2016).

[20] M. Otto, H. Feil, R. V. Woerden, J. Wijngaard, P. V. D. Valk, C. V. Bruggen, and C. Haas, J. Magn. Magn. Mater. **70**, 33 (1987).

[21] M. Terada, K. Endo, Y. Fujita, and R. Kimura, J. Phys. Soc. Jpn. **32**, 91 (1972).

[22] H. C. Kandpal, C. Felser, and R. Seshadri, J. Phys. D: Appl. Phys. **39**, 776 (2006).

[23] I. Skovsen, L. Bjerg, M. Christensen, E. Nishibori, B. Balke, C. Felser, and B. B. Iversen, Dalton Trans. **39**, 10154 (2010).

[24] J. Ma, V. I. Hegde, K. Munira, Y. Xie, S. Keshavarz, D. T. Mildebrath, C. Wolverton, A. W. Ghosh, and W. H. Butler, Phys. Rev. B **95**, 024411 (2017).

[25] C. B. Evers, C. G. Richter, K. Hartjes, and W. Jeitschko, J. Alloys Compd. **252**, 93 (1997).

[26] K. Buschow, P. van Engen, and R. Jongebreur, J. Magn. Magn. Mater. **38**, 1 (1983).

[27] J. Kubler, K. H. Hock, J. Sticht, and A. R. Williams, J. Phys. F: Met. Phys. **18**, 469 (1988).

[28] See http://www.openmx-square.org/ for "Openmx."

[29] J. P. Perdew, K. Burke, and M. Ernzerhof, Phys. Rev. Lett. **77**, 3865 (1996).

[30] N. Troullier and J. Martins, Phys. Rev. B **43**, 1993 (1991).

[31] G. Theurich and N. A. Hill, Phys. Rev. B **64**, 073106 (2001).

[32] T. Ozaki, Phys. Rev. B **67**, 155108 (2003).

[33] A. A. Mostofi, J. R. Yates, Y.-S. Lee, I. Souza, D. Vanderbilt, and N. Marzari, Comput. Phys. Commun. **178**, 685 (2008).

[34] J. M. Ziman, *Principles of the Theory of Solids*, 2nd ed. (Cambridge University Press, 1972).

[35] J. Tobola, J. Pierre, S. Kaprzyk, R. V. Skolozdra, and M. A. Kouacou, J. Phys.: Condens. Matter **10**, 1013 (1998).

[36] S. Ouardi, G. H. Fecher, C. Felser, M. Schwall, S. S. Naghavi, A. Gloskovskii, B. Balke, J. Hamrle, K. Postava, J. Pištora, S. Ueda, and K. Kobayashi, Phys. Rev. B **86**, 045116 (2012).

[37] Y. Xia, V. Ponnambalam, S. Bhattacharya, A. L. Pope, S. J. Poon, and T. M. Tritt, J. Phys.: Condens. Matter **13**, 77 (2001).

[38] J. Kübler and C. Felser, Phys. Rev. B **85**, 012405 (2012).

[39] J.-C. Tung and G.-Y. Guo, New J. Phys. **15**, 033014 (2013).

[40] X. Wang, J. R. Yates, I. Souza, and D. Vanderbilt, Phys. Rev. B **74**, 195118 (2006).